Ibn Al-Haitham Journal for Pure and Applied Sciences
Journal homepage: jih.uobaghdad.edu.iq
PISSN: 1609-4042, EISSN: 2521-3407
IHJPAS. 2026; 39(1)

Study of Nuclear Properties in the Exotic Mirror Nuclei ^{8}B and ^{8}Li

Ghufran M. Sallh[1*] and **Ahmed N. Abdullah**[2]
[1] Department of Physics, College of Science, University of Baghdad, Ibn Sina University, Baghdad, Iraq.
[2] Department of Physics, College of Science, University of Baghdad, Baghdad, Iraq
*Corresponding Author

Received: 8/August/2025.
Accepted:16/November/2025
Published: 20/January/2026.
doi.org/10.30526/39.1.4276

Abstract

The ground-state properties like the nuclear densities and the root mean square radii of exotic mirror nuclei ^{8}B and ^{8}Li have been investigated using the Skyrme Hartree Fock and Symmetrized woods Saxon calculations. Additionally, several nuclear observables have been investigated, including longitudinal elastic electron scattering form factors, binding energies, Coulomb displacement energies, magnetic dipole moments, and electric quadrupole moments. The results of the evaluation are contrasted with the experimental data that is currently available. It found that a common feature of the neutron and matter densities for the above-selected exotic nuclei is the long tail behavior. We assumed that both ^{8}Li and ^{8}B have a structure of the core nuclei ^{7}Be and ^{7}L plus a valence. It found that the structure of the valence one-neutron of ^{8}Li and one-proton ^{8}B is a pure $1p_{1/2}$ orbit. The elastic charge form factors of the above selected exotic nuclei are evaluated using the plane wave Born approximation and compared with those of their stable isotope ^{7}Li and ^{10}B.

Keywords: Mirror nuclei, Symmetrized Woods-Saxon potential.

1.Introduction

The investigation of short-lived nuclei far from the β-stability line has become a hot point in nuclear physics due to their unusual structural features and their role in advancing our understanding of nuclear forces and exotic [1, 2]. This has led to the discovery of neutron halos in light neutron-rich nuclei such as ^{6}He, ^{11}Li, and ^{14}Be. These halos result from weakly bound valence nucleons occupying low angular momentum states (l = 0 or 1), allowing their wave functions to extend significantly. A key characteristic of halo nuclei is the presence of a low-density tail in their matter distribution at large radial distances [3,4]. The fragment momentum distribution, total reaction cross-section Coulomb dissociation, and nuclear quadrupole are all experimental methods used in nuclear physics to extract information about nuclear structure, especially for exotic or unstable nuclei. These methods can help identify the properties of nuclear halos and skins, as well as determine other nuclear properties like size and shape [5, 6]. Additional information on the nuclear structure can be obtained by the proton elastic scattering at intermediate energies. It gives insights into both the nuclear-matter density distribution and the nuclear-matter radius. This technique is well-established for the study of stable nuclei and may also be used to investigate unstable nuclei when applied to inverse kinetics with radiation beams [7].One of the classic problems in nuclear structure physics is to understand the displacement energies of nuclei. The displacement energy is the binding energy difference between mirror nuclei (those with the same mass number A but with the proton Z and neutron N numbers interchanged). If the nuclear. Force is charge symmetric, then this binding energy difference can be related to the well-understood Coulomb interaction between the protons [8]. In addition, a rather interesting feature of studying the mirror nuclei is that the neutron skin thickness can be found through the knowledge of proton radii alone from the mirror pairs. It has recently been proposed that the difference between the charge radii of mirror nuclei is proportional to the neutron skin [9].

The ground-state properties, including nuclear densities and rms radii, of exotic mirror nuclei ^{8}B and ^{8}Li were investigated using Skyrme-Hartree-Fock (SHF) and symmetrized Woods-Saxon (SWS) models. Their longitudinal and transverse elastic form factors($|F_L(q)|^2$), as well as electric quadrupole (Q) and magnetic dipole (μ) moments, were also studied.

2.Materials and Methods

The nucleon density of exotic nuclei is given by the following expression [2]:

$$\rho_m(r) = \rho_c(r) + \rho_v(r) \quad (1)$$

Where $\rho_c(r)$ (core density) and $\rho_h(r)$ (halo density) are expressed as [2]:

$$\rho_c(r) = \frac{1}{4\pi}\sum_{n\ell j} N_c^{n\ell j}\,|R_{n\ell j}(r)|^2 \quad (2)$$

$$\rho_h(r) = \frac{1}{4\pi} N_h^{n\ell j}|R_{n\ell j}(r)|^2 \quad (3)$$

Where $R_{n\ell j}(r)$ and $N^{n\ell j}$ denote radial wave function and occupation number of the orbit $n\ell j$, respectively.

The $R_{n\ell j}(r)$ was obtained by solving the radial Schrödinger equation with the SWS potential [2]:

$$\frac{d^2R_{n\ell j}(r)}{dr^2} + \frac{2m}{\hbar^2}\left[\varepsilon_{n\ell j} - V(r) - \frac{\hbar^2}{2m}\frac{\ell(\ell+1)}{r^2}\right]R_{n\ell j}(r) = 0 \quad (4)$$

Where $\varepsilon_{n\ell j}$ is the single-particle binding energy and the $V(r)$ is the core potential given as [2]:

$$V(r) = V_0(r) + V_{so}(r)\,\boldsymbol{L.S} + V_c(r) \quad (5)$$

$V_0(r)$ is the central potential takes the SWS from [10]:

$$V_0(r) = -V_0\,\frac{1+\sinh(R_0/a_0)}{\cosh(r/a_0)+\cosh(R_0/a_0)} \quad (6)$$

$V_{so}(r)$ is spin orbit potential [2]:

$$V_{so}(r) = V_{so}\frac{1}{r}\left[\frac{d}{dr}\frac{1}{(1+e^{(r-R_{so})/a_{so}})}\right] \quad (7)$$

$V_c(r)$ (for protons only) is the Coulomb potential [11]:

$$V_c(r) = \begin{cases} \dfrac{Ze^2}{r} & \text{for} \quad r > R_c \\ \dfrac{Ze^2}{R_c}\left[\dfrac{3}{2} - \dfrac{r^2}{2R_c^2}\right] & \text{for} \quad r \le R_c \end{cases} \quad (8)$$

and $V_c(r) = 0$ for neutrons.

The Skyrme force are given by [1]:

$$V_{Skyrme} = \sum_{i<j} V_{ij} = t_0(1+x_0P_\sigma)\delta(\vec{r}) + \frac{t_1}{2}(1+x_1P_\sigma)\left[\delta(\vec{r})\vec{k}^2 + \vec{k}'^2\delta(\vec{r})\right] + t_2(1+x_2P_\sigma)\overrightarrow{k'}.\delta(\vec{r})\vec{k} + \frac{1}{6}t_3(1+x_3P_\sigma)\rho^\alpha(\vec{R})\delta(\vec{r}) + it_4\vec{k}'.\delta(\vec{r})(\vec{\sigma}_i+\vec{\sigma}_j) \times \vec{k}\,, \quad (9)$$

where $P_\sigma, \vec{\sigma}$, $\delta(\vec{r})$ and $\vec{k}$ are the space exchange operator, Pauli spin matrix vector, delta function pairing force, and the relative momentum, respectively and t_0, t_1, t_2, t_3, x_0, x_1, x_2, x_3, W_0 and γ are the parameters of the Skyrme force.

The charge, as well as the densities of protons or neutrons with the range of the Skyrme HF methodology, are obtained as [12]:

$$\rho_g(\vec{r}) = \sum_{\beta\in g} w_\beta\psi_\beta^+(\vec{r})\,\psi_\beta(\vec{r})\,, \qquad g = n,p,ch \quad (10)$$

The coefficient ψ_β denotes the occupation probability of the single-particle quantum state β. It reflects the likelihood that the state is occupied by a nucleon (proton or neutron).
The nuclear charge distribution ($\rho_{ch}(r)$) was obtained using the folding relation [2]:

$$\rho_{ch}(r) = \int \rho_p(r) f_p(r' - r)\, dr', \qquad (11)$$

Where $\rho_p(r)$ is the proton density and f_p the intrinsic charge distribution of a proton.
Where f_p takes the following form of Gaussian [2]:

$$f_p(r) = \frac{1}{\left(\sqrt{\pi} a_p\right)^3} e^{\left(-r^2/a_p^2\right)} \qquad (12)$$

a_p is a range parameter in the Gaussian function used to model the proton's charge distribution.
The core (R_c), matter (R_m), proton $\left(R_p\right)$ and neutron (R_n) RMS radii are obtained by as follow [13]:

$$R_g = \langle r_g^2 \rangle^{1/2} = \left[\frac{\int r^2 \rho_g(r) dr}{\int \rho_g(r) dr}\right]^{1/2} \qquad g = c, m, n, p, ch \qquad (13)$$

The proton and neutron skin thicknesses are, respectively [14]:

$$\Delta R_p = R_p(Z, N) - R_n(Z, N) \qquad (14)$$

$$\Delta R_n = R_n(Z, N) - R_p(Z, N) \qquad (15)$$

We have in mirror nuclei with assumed that perfect charge symmetry [14]:

$$R_n(Z, N) = R_p(Z, N) \qquad (16)$$

Then, the difference of the proton radii of the mirror pair is [14]:

$$\Delta R_{mirror} = R_p(N, Z) - R_p(Z, N) \qquad (17)$$

In plane the wave Born approximation (PWBA), the elastic charge form factor ($F_{ch}(q)$) is given by [15]:

$$F_{ch}(q) = \frac{4\pi}{Z} \int_0^\infty \rho_{ch}(r) j_0(qr) r^2 dr, \qquad (18)$$

Where $j_0(qr)$ denotes the Bessel function and q the momentum transfer.
The longitudinal, transverse electric and transverse magnetic form factors between nuclear states J_i and J_f are given by [16]:

$$\left|F_J^\eta(q)\right|^2 = \frac{4\pi}{Z^2(2J_i + 1)} \sum_J \left|\langle J_f \| \hat{T}_J^\eta(q) \| J_i \rangle\right|^2 \qquad (19)$$

Where η refers to the type (longitudinal, transverse magnetic or transverse electric).
The Q in terms of the E2 operator is defined as [17]:

$$Q = \sqrt{\frac{16\pi}{5}} \begin{pmatrix} J & 1 & J \\ -J & 0 & J \end{pmatrix} \sum_{t_z} \left|\langle J \| \hat{O}(E2)_{t_z} \| J \rangle\right|^2 e_{t_z} \qquad (20)$$

The μ in terms of the M1 operator is defined as [18]:

$$\mu = \sqrt{\frac{4\pi}{3}} \begin{pmatrix} J & 1 & J \\ -J & 0 & J \end{pmatrix} \sum_{t_z} \left|\langle J \| \hat{O}(M1)_{t_z} \| J \rangle\right|^2 \mu_N \qquad (21)$$

Where μ_N is the nuclear magneton.

3. Results

In this study, we have been calculated the nuclear proton, neutron and matter densities, the corresponding rms radii, the elastic longitudinal ($|F_L(q)|^2$) and transverse ($|F_T(q)|^2$) form factors along with the electric and magnetic dipole moments for exotic mirror nuclei ^{8}B (S_{1p}=0.136 MeV, $\tau_{1/2}$=770 ms) and ^{8}Li (S_{1n}=2.032 MeV, $\tau_{1/2}$=839.4 ms) [19,20] using the SHF and SWS calculations. The LNS5 Skyrme parameterization has been used within the SHF calculations in this work. The values of the LNS5 parameterization employed in our calculations are $t_0 = -2194.776$, $t_1 = 482.518$,

$t_2 = 138.137,\ t_3 = 10784.169,\ x_0 = 0.134,\ x_1 = -0.097,\ x_2 = -1.399,\ x_3 = 0.171,\ W_0 = 105.674,\ \gamma = 0.16667$ [21]. A core ^{7}Be (J^π,T=3/2$^-$,1/2) with configuration $\{(1s_{1/2})^4, (1p_{3/2})^3\}$plus a proton structure is assumed for ^{8}B (J^π,T=2$^+$,1) and a core ^{7}Li (J^π,T=3/2$^-$,1/2) with configuration $\{(1s_{1/2})^4, (1p_{3/2})^3\}$with a neutron structure is assumed for ^{8}Li (J^π,T=2$^+$,1). The valence proton in ^{8}B (valence neutron in ^{8}Li) was assumed to be a pure $1p_{1/2}$ orbit.

Table 1. The SWS parameters [22]

Nuclei	V_0 (MeV)		V_{so} (MeV)	$a_0 = a_{so}$ (fm)	$r_0 = r_{so}$ (fm)	r_c (fm)
	Core	Valence				
^{8}B	60.491	39.64	6.0	0.548	1.458	1.511
^{8}Li	60.491	37.02	6.0	0.485	1.486	1.511
^{7}Li	49.378		6.0	0.411	1.321	1.533
^{10}B	48.606		6.0	0.494	1.307	1.477

Table 2. The calculated ε together with that of Ref. [22] as well as experimental data [20]

Nuclei	$n\ell_j$	proton			neutron		
		ε_{cal} (MeV)	ε(MeV) [22]	$\varepsilon_{exp.}$(MeV)[20]	ε_{cal} (MeV)	ε(MeV)[22]	$\varepsilon_{exp.}$(MeV)[20]
^{8}B	$1s_{1/2}$	−33.322	−33.322	-----	−35.798	−35.798	-----
	$1p_{3/2}$	−16.592	−16.592	-----	−18.819	−18.819	-----
	$1p_{1/2}$	−0.136	-----	−0.136	-----	-----	-----
^{8}Li	$1s_{1/2}$	−36.161	−36.161	-----	−36.267	−36.267	-----
	$1p_{3/2}$	−19.340	−19.340	-----	−19.757	−19.757	-----
	$1p_{1/2}$	-----	-----	-----	−2.032	-----	−2.032

Table 3. The calculated $R_c$and R_m rms radii and experimental ones

Nuclei	R_c			R_m		
	SHF	SWS	Exp. [23,24]	SHF	SWS	Exp. [24,25]
^{8}B	2.26	2.27	2.31±0.02	2.55	2.55	2.55±0.08
^{8}Li	2.27	2.27	2.33±0.02	2.50	2.50	2.50±0.06

Table 4. The calculated R_p and R_n rms radii and experimental ones

Nuclei	R_p			R_n		
	SHF	SWS	Exp. [23,24]	SHF	SWS	Exp. [24,25]
^{8}B	2.74	2.73	2.76±0.04	2.20	2.18	2.16±0.03
^{8}Li	2.20	2.18	2.16±0.04	2.66	2.66	2.66±0.11

Table 5. Calculated $\Delta R_p, \Delta R_n$ and ΔR_{mirror} of ^{8}B and ^{8}Li

Nucleus	ΔR_p		Mirror	ΔR_n		ΔR_{mirror}	
	SHF	SWS		SHF	SWS	SHF	SWS
^{8}B	0.54	0.55	^{8}Li	0.46	0.48	-0.54	-0.55

Table 6. Calculated and experimental results of Q moment.

Nuclei	PMOM	PJP	CKII	PJT	Exp. [26-28]
^{8}B	3.67	4.39	4.20	4.51	6.30±0.05
^{10}B	9.08	9.44	9.12	9.40	8.47±0.06
^{8}Li	2.60	2.95	2.64	3.14	3.17±0.02
^{7}Li	-3.86	-3.80	-3.85	-3.78	-3.70±0.08

Table 7. Calculated and experimental results of μ moment.

Nuclei	PMOM	PJP	CKII	PJT	Exp. [26,29,30]
^{8}B	1.019	1.225	1.298	1.176	1.03±0.003
^{10}B	1.822	1.836	1.811	1.830	1.80±0.006
^{8}Li	1.611	1.451	1.377	1.495	1.65±0.002
^{7}Li	3.26	3.21	3.235	3.206	3.25±0.002

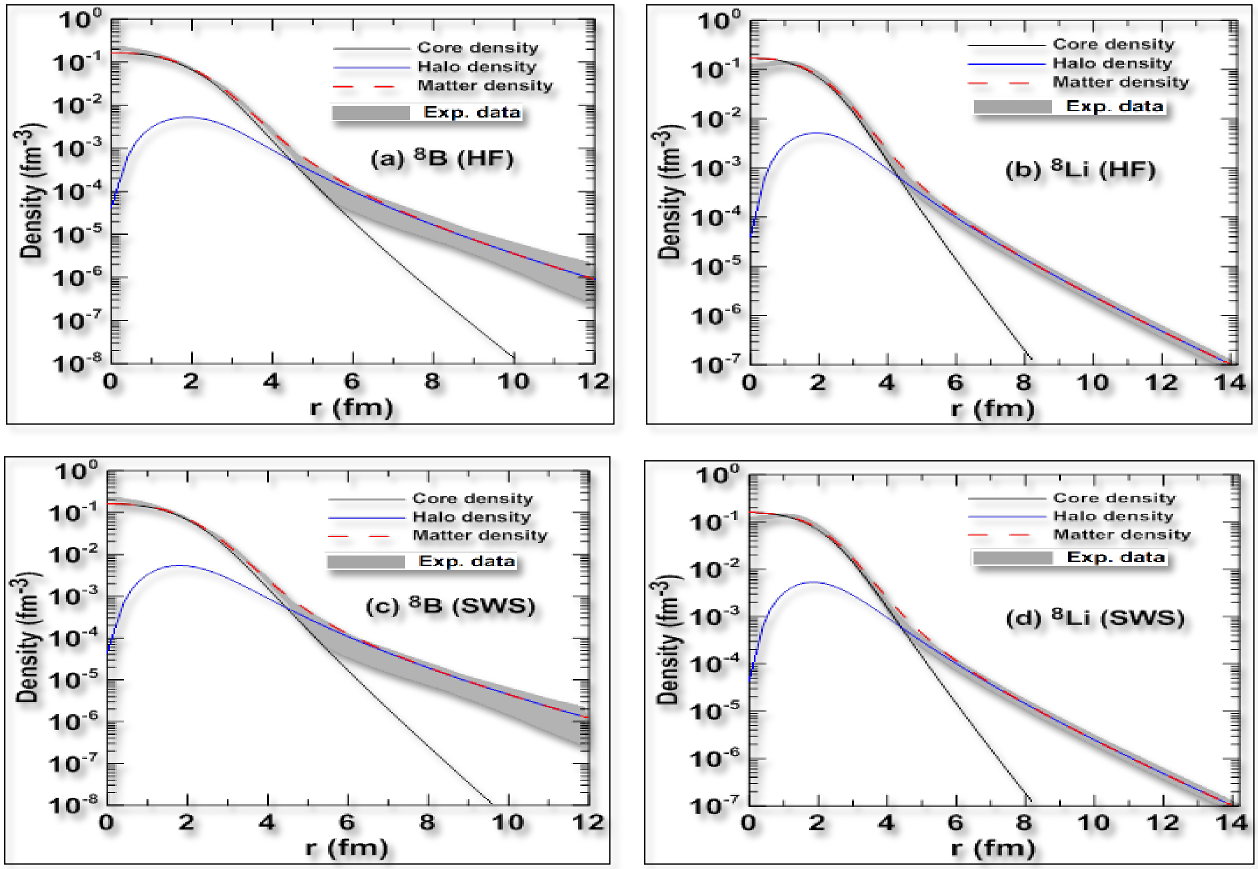

Figure 1. The core, halo and matter density distributions of exotic mirror nuclei ^{8}B and ^{8}Li.

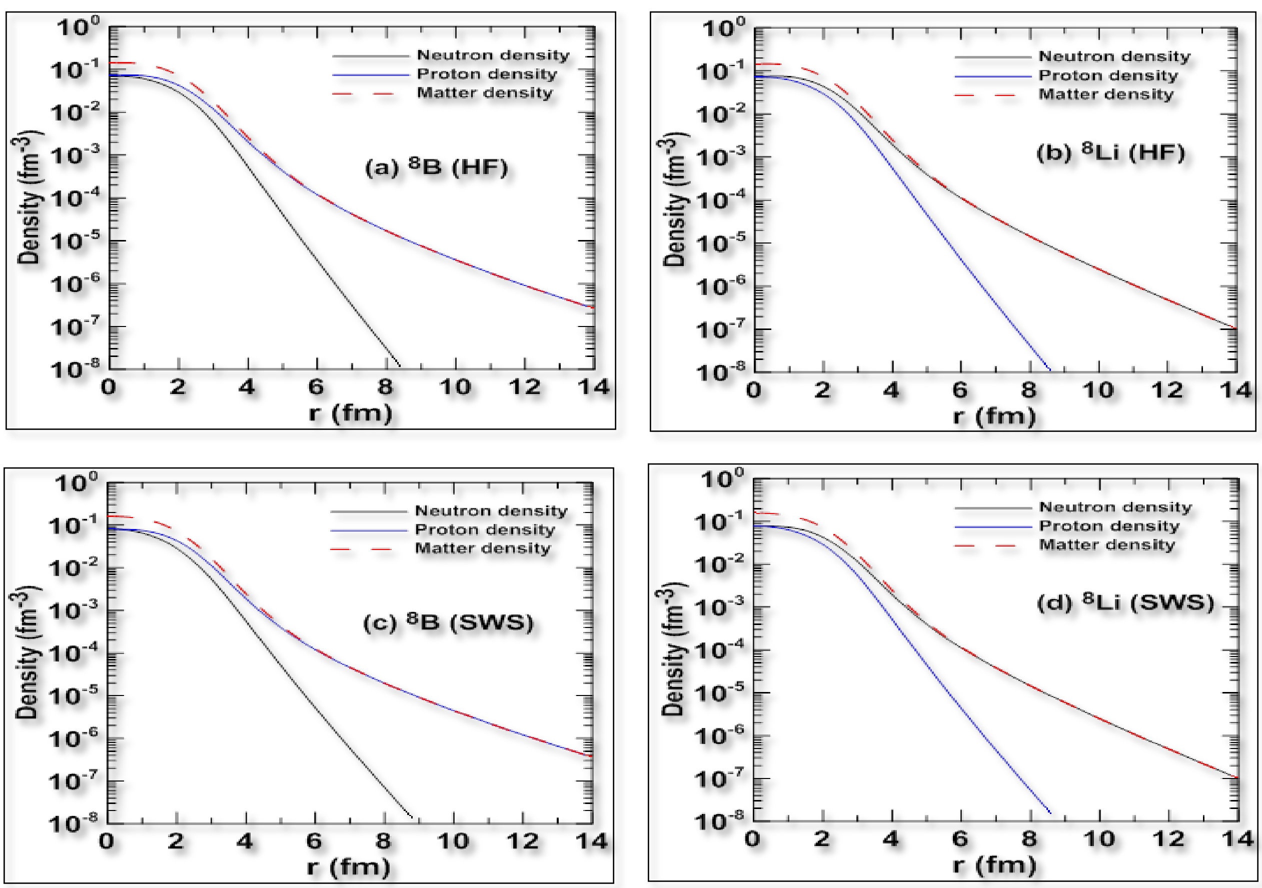

Figure 2. The proton, neutron and matter density distributions of exotic mirror nuclei ^{8}B and ^{8}Li.

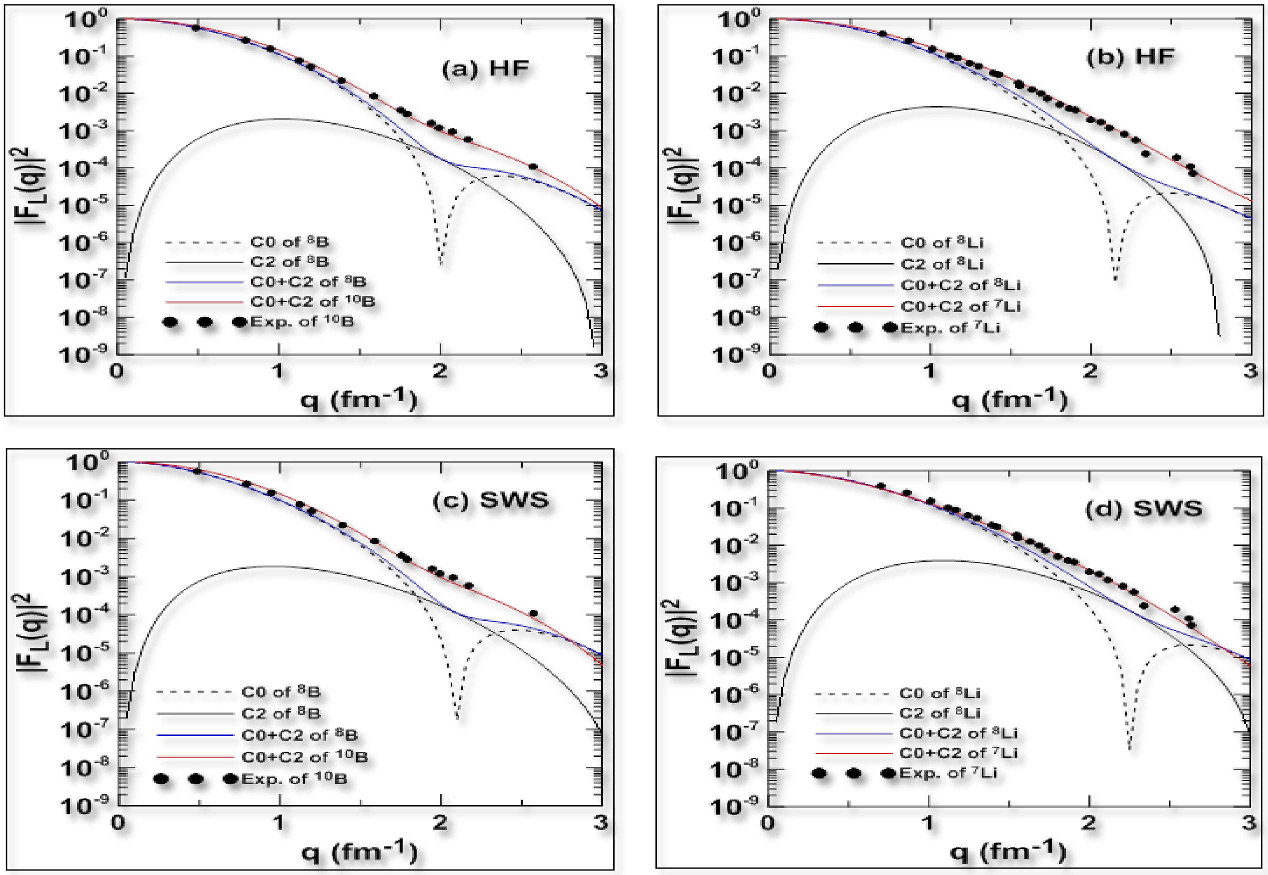

Figure 3. The longitudinal form factors of the isotopes ^{10,8}B and ^{7,8}Li.

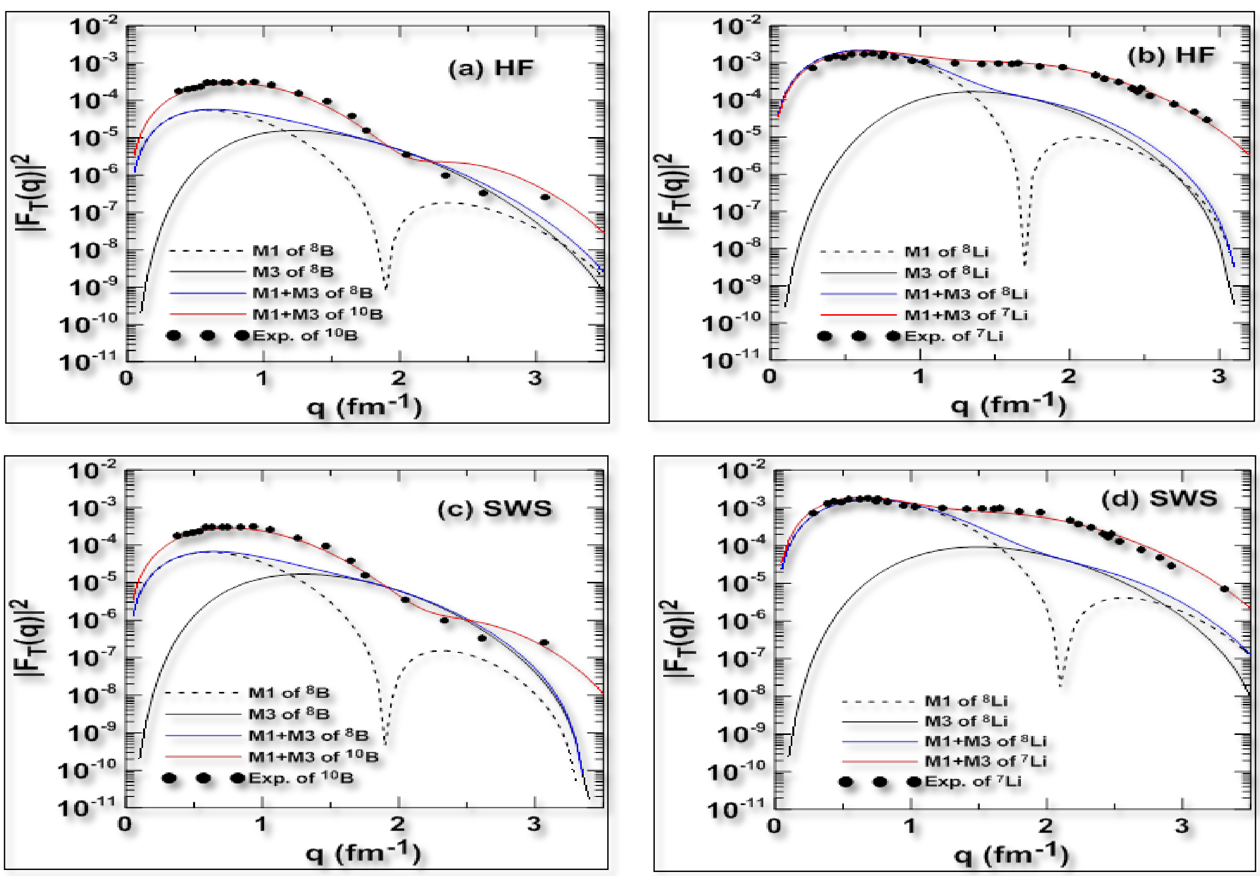

Figure 4. The transverse form factors of the isotopes ^{10,8}B and ^{7,8}Li.

4.Discussion

The values of the SWS parameters utilized in the present calculations for the selected nuclei and showed in **Table 1**. The potential depth for neutrons (V_0^n) and protons $\left(V_0^p\right)$ in core nuclei has been used the default of the NushellX@MSU program [22], where the V_0^n for valence neutron and other parameters, provide the experimental ε of the last neutron as well as the matter rms radius of the halo nuclei.

The calculated $\varepsilon_{n\ell j}$ for proton and neutron is listed in **Table 2**. Due to the absence of the available experimental single particle energies for core nuclei, the experimental data is given for the last proton and neutron only.

Tables 3 and **4** present the core (R_c), matter (R_m), proton $\left(R_p\right)$ and neutron (R_n) rms radii (in fm) of selected mirror nuclei obtained by the SHF and SWS calculations. The corresponding experiment rms radii [23-25] are also given in these tables for comparison purposes. From these tables, we noted that the calculated results of our present study agree reasonably within the quoted error with the experimental results.

Table 5 shows the calculated proton skin of halo nucleus ^{8}B and the neutron-skin of its mirror nucleus ^{8}Li as well as the difference of proton radii for these mirror pair obtained by the SHF and SWS calculations. It can be seen from Table 5 that the proton skin of the proton-rich nucleus ^{8}B is larger than the neutron skin of its mirror neutron-rich nucleus ^{8}Li. This is attributed to the Coulomb repulsion of protons.

The calculated Q and μ moments for ^{10,8}B and ^{7,8}Li isotopes are presented in **Tables 6** and **7.** respectively, together with the experimental data [26-30]. These calculations were performed using the p-model space with different interactions labeled as PMOM, CKII, PJP and PJT. The effective charges of the NuShellX@MSU code $\left(e_p^{eff} = 1.5\,e, e_n^{eff} = 0.5e\right)$ are used to calculate the quadrupole moment. Free-nucleon g factors are used for calculating the dipole moments. From **Table 6** it can be seen that the calculated quadrupole moment for ^{8}B obtained by all interactions are underestimates the measured value (6.30±0.05). The sign is correctly reproduced. For ^{10}B all calculations overestimate the measured value (8.47±0.06) with the correct sign. Calculations of ^{8}Li with PJT interaction give the value of the quadrupole moment (3.17) which is in a very good agreement with the experimental value (3.14±0.02) in sign and magnitude. The experimental value of ^{7}Li (-3.70±0.08) is very well reproduced by PJT interaction (-3.78) within its error. Calculations predict a negative sign as the measured value. The measured quadrupole moment for ^{8}B is about twice that of the ^{8}Li. This large enhancement of the quadrupole moment of ^{8}B indicates a large deformation in comparison with that of ^{8}Li, its mirror nucleus. It can be shown from **Table7.** that the measured magnetic moment for ^{8}B (1.03±0.003) is very well reproduced by PMOM interaction (1.019) in sign and magnitude. For ^{10}B, all calculations are in an excellent agreement with the measured value (1.80±0.006) within the experimental error. Calculations predict a positive sign as the measured value. The experimental value (1.65±0.002) of ^{8}Li is very good reproduced by the PMOM interaction (1.611), while it is underestimated with other interactions. The sign is correctly reproduced. The magnetic moment for ^{7}Li (3.25±0.004) is very well explained by all calculations.

In **Figure 1** we present the calculated matter densities obtained by both the SHF (left part) and SWS (right part) of the mirror nuclei ^{8}B **[Figures 1(a) and 1(c)] and ^{8}Li [Figs. 1(b) and 1(d)]** and compared them with experimental densities (grey area). The experimental data of ^{8}B and ^{8}Li are taken from Refs. [1] and [31] correspondingly. In these figures the black and blue curves represent the calculated results of the core and halo densities, respectively. For both mirror nuclei a good description of the experimental matter densities is attained with both calculations which exhibit an extended halo. In ^{8}B, the proton rich nucleus, the halo density extends further outward, indicating a more pronounced "proton halo." This is due to the very low binding energy of the valence proton in ^{8}B (S_{1p} = 0.136 MeV), which allows its wavefunction to spread significantly outside the nuclear core. In contrast, ^{8}Li, which is neutron-rich, shows a less extended tail for the neutron halo, consistent with its higher neutron separation energy (S_{1n} = 2.032 MeV).

Figure 2 depict the neutron, proton and matter densities displayed as black , blue and dashed-red distributions, respectively for exotic ^{8}B-^{8}Li mirror nuclei. It is clearly shown from the left panel of these figures that a long tail exists in the proton density distributions of ^{8}B, which supports the proton halo structure for these nuclei. Moreover, the difference between the proton and neutron rms radii ($R_p - R_n$) of ^{8}B are 0.54 fm obtained by SHF and SWS calculations, respectively. This difference gives an extra support for the proton halo structure of ^{8}B. On the contrary, it can be seen from the right panel of **Figure 3** that the long-tail performance is clearly noticed in the neutron densities of ^{8}Li, which supports the neutron halo structure for these nuclei. In addition, the difference between the neutron and proton rms radii ($R_n - R_p$) of ^{8}Li are 0.46 and 0.48 fm obtained by SHF and SWS calculations, respectively This difference gives an extra support for the neutron halo structure of ^{8}Li.
The total longitudinal charge form factors (C_0+C_2) for ^{10,8}B and ^{7,8}Li, isotopes calculated by the SHF and SWS methods are displayed in **Figure 3** along with the experimental charge form factors (dotted symbols) of the stable isotopes ^{10}B [32] and ^{7}Li [33]. Therein, the form factors C_0+C_2 of unstable (halo) and stable isotopes are portrayed by the blue and red curves, respectively. The C_0 and C_2 components of unstable nuclei form factors are given by the dashed and black curves, respectively.in these figures the top panel correspond to nuclei pairs ^{10,8}B and ^{7,8}Li. Calculations of the OBDM elements are performed with *p*-model space using PMOM interaction which are carried out via the NuShellX@MSU code[22]. The level of agreement between the results of our calculations for stable nuclei ^{10}B and ^{7}Li with the experimental data is very good. Although the number of the protons within a given pair of isotopes is the same, the charge form factors are quite different from each other. One can see from **Figures 3a** and **3c** that the form factors of ^{8}B decreases faster than that of ^{10}B with increasing momentum transfer. This change is due to the influence of the charge density of the outer proton in ^{8}B. As with the longitudinal form factors of ^{8}B, the addition of neutron to ^{8}Li pull the charge density out and thus the form factors decrease with momentum transfer as shown in **Figures 3b** and **3d**.
Figure 4 compare the total transverse elastic form factors (M1+M3) of ^{10,8}B (left panel) and ^{7,8}Li (right panel) isotopes calculated using the SHF and SWS methods. The blue and red curves refer to M1+M3 of unstable and stable isotopes, respectively. While the M1 and M3 components for unstable ^{8}Li and ^{8}B nuclei are given by the dashed and black curves, respectively. For comparison the experimental charge form factors of stable isotopes ^{10}B [34] and ^{7}Li [33] are given by dotted symbols. The agreement of theoretical results with the experimental data for the stable isotopes^{10}B and ^{7}Li is very well. The effect of the neutron (proton) halo on this form factor for ^{8}Li (^{8}B) is just as dramatic as that on the longitudinal one. It can be seen from these figures; the blue curve decreases faster than the red curve with increasing momentum transfer. As with the longitudinal form factor, that decrease is due to the influence of the charge density of the outer proton in ^{8}B and due to the coupling of the extra neutron to the ^{7}Li core.

5.Conclusion

The ground-state properties like the nuclear densities and the rms radii for exotic neutron-rich nuclei ^{8}B and ^{8}Li have been investigated in the framework of the SHF and SWS calculations. The evaluated results are compared with available experimental data. This study draws the following conclusions:
It is found that both the SHF and SWS calculations are capable of providing theoretical predictions on the structure of exotic nuclei (considered in this study) and provide a satisfactory description of experimental data.
The halo structure of the above exotic nuclei is emphasized through exhibiting the long tail performance in their calculated matter density distributions, where this performance is considered a distinctive feature of halo nuclei.
The elastic $|F_L(q)|^2$and $|F_T(q)|^2$ form factors for the ^{10,8}B and ^{7,8}Li isotopes have also been studied. Calculations of the OBDM elements were performed with *p*-model space using the PMOM

interaction, which was carried out via the NuShellX@MSU code. It was found that, the $|F_L(q)|^2$and $|F_T(q)|^2$ form factors of exotic nuclei decreased faster than those of stable isotopes with increasing q. The calculated results of the nuclear quadrupole (Q) and magnetic dipole (μ) moments using the shell model calculations within the effective interactions show a reasonable agreement with the experimental values.

Acknowledgment

We sincerely thank my supervisor, [Ahmed N. Abdullah], for his invaluable guidance and academic support throughout this work.

Conflict of Interest

The author declares no conflicts of interest.

Funding

No external funding supported this work.

Ethical Clearance

As a theoretical study with no human or animal subjects, ethical approval was unnecessary.

References

1. Abdullah AN. Systematic study of the nuclear structure for some exotic nuclei using Skyrme–Hartree–Fock method. Iran J Sci Technol Trans Sci. 2020;44:283–288. https://doi.org/10.1007/s40995-019-00799-x
2. Abdullah AN, Flaiyh GN. Study of density distributions for some exotic nuclei using symmetrized Woods–Saxon potential. Mod Phys Lett A. 2020;40:2550036. https://doi.org/10.1142/S0217732325500361
3. Hansen PG, Jonson B. The neutron halo of extremely neutron-rich nuclei. Eur Phys Lett. 1987;4(4):409–414. https://doi.org/10.1209/0295-5075/4/4/005
4. Wang Z, Ren ZZ. Probing proton halo of the exotic nucleus 28S by elastic electron scattering. Sci China Ser G Phys Astron. 2004;47:42–51. https://doi.org/10.1360/02yw0187
5. Nakamura T, Fukuda N, Kobayashi T, Aoi N, Iwasaki H, Kubo T, Mengoni D, Notani M, Saito T, Shimoura S, Suzuki T, Takahashi H, Yanagisawa Y, Ishihara M. Coulomb dissociation of 19C and its halo structure. Phys Rev Lett. 1999;83(6):1112–1115. https://doi.org/10.1103/PhysRevLett.83.1112
6. Geithner W, Kappertz S, Keim M, Lievens P, Neugart R, Neyens G, Vermeeren L, Vingerhoets P, Wilbert J. Measurement of the magnetic moment of the one-neutron halo nucleus 11Be. Phys Rev Lett. 1999;83:3792–3795. https://doi.org/10.1103/PhysRevLett.83.3792
7. Alkhazov GD, Belostotsky SL, Vorobyov AA. Scattering of 1 GeV protons on nuclei. Phys Rep. 1978;42:89–144. https://doi.org/10.1016/0370-1573(78)90083-2
8. Tu XL, Zhang YH, Xu XH, Wang M, Audi G. A survey of Coulomb displacement energies and anomalous behavior in the upper fp-shell. J Phys G Nucl Part Phys. 2014;41:025104. https://doi.org/10.1088/0954-3899/41/2/025104
9. Kumar P, Kaur S, Thakur V, Kumar R, Dhiman SK. Neutron skin thickness and proton radii of mirror nuclei within covariant density functional theory. Mod Phys Lett A. 2024;39(07):2450022. https://doi.org/10.1142/S0217732324500226
10. Grypeos ME, Koutroulos CG, Papadopoulos HM. The “cosh” or symmetrized Woods–Saxon nuclear potential. J Phys G Nucl Part Phys. 1991;17:1093–1105. https://doi.org/10.1088/0954-3899/17/7/008
11. Chu Y, Ren ZZ, Xu C. Properties of proton-rich nuclei in a three-body model. Eur Phys J A. 2008;37:361–366. https://doi.org/10.1140/epja/i2008-10626-2
12. Abbas SA, Raheem EM, Alwan IH. Nuclear structure of some Ni and Zn isotopes with Skyrme–Hartree–Fock interaction. Baghdad Sci J. 2022;19:914–923. https://doi.org/10.21123/bsj.2022.19.4.0914
13. Raheem EM, Abdul Hasan AA, Alwan IH. Ground state properties of some Ni isotopes using Skyrme–Hartree–Fock method. Iraqi J Phys. 2019;17:1–10. https://doi.org/10.30723/ijp.v17i42.195
14. Sammarruca F. Proton skins, neutron skins, and proton radii of mirror nuclei. Front Phys. 2018;6:8. https://doi.org/10.3389/fphy.2018.00090
15. Antonov AN, Gaidarov MK, Kadrev DN, Hodgson PE, De Guerra EM. Charge density distributions and

form factors in neutron-rich exotic nuclei. Int J Mod Phys E. 2004;13:759–782. https://doi.org/10.1142/S0218301304002430

16. Karataglidis S, Amos K. Electron scattering form factors from exotic nuclei. Phys Lett B. 2007;650:148–152. https://doi.org/10.1016/j.physletb.2007.04.051
17. Ali AH. Electric quadrupole moments of some scandium isotopes using shell model calculations. Baghdad Sci J. 2018;15:304–310. https://doi.org/10.21123/bsj.2018.15.3.0304
18. Brussaard PJ, Glaudemans PWM. Shell Model Applications in Nuclear Spectroscopy. Amsterdam: North-Holland; 1977.
19. Audi G, Kondev FG, Wang M, Huang WJ, Naimi S. The NUBASE2016 evaluation of nuclear properties. Chin Phys C. 2017;41(3):030001. https://doi.org/10.1088/1674-1137/41/3/030001
20. Wang M, Huang WJ, Kondev FG, Audi G, Naimi S. AME 2020 atomic mass evaluation (II). Chin Phys C. 2021;45:030003. https://doi.org/10.1088/1674-1137/abddaf
21. Gambacurta D, Li L, Colò G, Lombardo U, Van Giai N, Zuo W. Local energy density functionals from Brueckner–Hartree–Fock calculations. Phys Rev C. 2011;84:024301. https://doi.org/10.1103/PhysRevC.84.024301
22. Brown BA, Rae WDM. The shell-model code NuShellX@MSU. Nucl Data Sheets. 2014;120:115–118. https://doi.org/10.1016/j.nds.2014.07.022
23. Tanihata I, Savajols H, Kanungo R. Experimental progress in nuclear halo structure studies. Prog Part Nucl Phys. 2013;68:215–313. https://doi.org/10.1016/j.ppnp.2012.07.001
24. Dobrovolsky AV, Korolev GA, Inglessi AG, Alkhazov GD, Colò G, Dillmann I, Yatsoura VI. Nuclear-matter distribution in 7Be and 8B. Nucl Phys A. 2019;989:40–58. https://doi.org/10.1016/j.nuclphysa.2019.05.012
25. Alkhazov GD, Vorobyov AA, Dobrovolsky AV, Inglessi AG, Korolev GA, Khanzadeev AV. Structure of light exotic nuclei by proton elastic scattering. Phys At Nucl. 2015;78:381–394. https://doi.org/10.1134/S1063778815020076
26. Stone NJ. Table of nuclear magnetic dipole and electric quadrupole moments. At Data Nucl Data Tables. 2005;90:75–176. https://doi.org/10.1016/j.adt.2005.04.001
27. Nesbet RK. Atomic Bethe–Goldstone calculations of hyperfine structure of B. Phys Rev A. 1970;2(4):1208–1213. https://doi.org/10.1103/PhysRevA.2.1208
28. Dubbers D, Dörr K, Ackermann H. Quadrupole moment of 8Li from NMR transitions. Z Phys A. 1977;282:243–252. https://doi.org/10.1007/BF01414890
29. Winnacker A. Narrow NMR lines of 8Li in solids. Phys Lett A. 1978;67:423–426. https://doi.org/10.1016/0375-9601(78)90353-5
30. Beckmann K, Boklen KD, Elke D. Magnetic dipole moments of light nuclei. Z Phys. 1974;270:173–182. https://doi.org/10.1007/BF01680407
31. Fan GW, Fukuda M, Nishimura D, Cai XL, Fukuda S, Hachiuma I, Ichikawa C, Izumikawa T, Kanazawa M, Kitagawa A, Kuboki T, Lantz M, Mihara M, Nagashima M, Namihira K, Ohkuma Y, Ohtsubo T, Ren ZZ, Sato S, Sheng ZQ, Sugiyama M, Suzuki S, Suzuki T, Takechi M, Yamaguchi T, Xu W. Phys Rev C. 2015;91:014614. https://doi.org/10.1103/PhysRevC.91.014614
32. Stovall T, Goldemberg J, Isabelle DB. Coulomb form factors of 10B and 11B. Nucl Phys. 1966;86:225–240. https://doi.org/10.1016/0029-5582(66)90302-6
33. Lichtenstadt J, Alster J, Moinester MA, Dubach J, Hicks RS, Peterson GA, Kowalski S. Form factors of the 7Li ground-state doublet. Phys Lett B. 1989;219:394–398. https://doi.org/10.1016/0370-2693(89)91083-6
34. Booten JGL, Van Hees AGM. Magnetic electron scattering from p-shell nuclei. Nucl Phys A. 1994;569:510–522. https://doi.org/10.1016/0375-9474(94)90316-6